Dendrite-Free Mg-MOF-Based All-Solid-State Lithium Metal Batteries with Superior Cycle Life

Xu-Dong Chen, Si Zhao, Xin-Fu Feng , Jin Huang , Yan Wang , Zhen-Chun Qiu, Jian-Biao Wang, Yi-Yin Huang , Li-Tuo Zheng*, Ming-Deng Wei, Zhen-Sheng Hong*

Abstract The widespread application of solid-state polymer electrolytes (SPE) is impeded due to their limited ionic conductivity, narrow electrochemical window, and lithium dendrite problem.

In this work, Mg-MOF is incorporated into a polyethylene oxide (PEO)-based polymer solid electrolyte, leading to the in-situ formation of LiF and other compounds at the electrolyte interface. This modification significantly improves lithium ion transport capabilities and regulates lithium deposition behavior, suppressing the formation of lithium dendrites. Mg-MOF serves as a Lewis acid site, facilitating anion adsorption and promoting the dissociation of LiTFSI, while also providing additional sites for complexation/decomplexation of lithium ions. As a result, symmetric Li//Li cells demonstrate stable plating/stripping performance for over 3000 hours with a low overpotential of 35 mV at 0.1 mA cm^{-2}. SPE@Mg-MOF exhibits high ionic conductivity (5.2×10^{-4} S cm^{-1} at 60 °C) and a high lithium ion migration number (0.64). Consequently, Li/SPE@Mg-MOF/$LiFePO_4$ full-cell demonstrates a high discharge capacity of 169.4 mAh g^{-1} at 0.1 C, a significantly improved rate capability with 145.7 mAh g^{-1} at 5 C, and an impressive capacity retention rate of 80% after stable cycling for 500 cycles at 1 C.

Keywords Solid state battery; Lithium metal; Polymer electrolytes; Mg-MOF

Supplementary Information The online version contains supplementary material available at…

Xu-Dong Chen and Si Zhao contributed equally to this work.

Xu-Dong Chen, Si Zhao, Xin-Fu Feng , Jin Huang , Yan Wang , Zhen-Chun Qiu, Yi-Yin Huang , Li-Tuo Zheng*, Zhen-Sheng Hong*
Fujian Provincial Key Laboratory of Quantum Manipulation and New Energy Materials, College of Physics and Energy, Fujian Normal University, Fuzhou, Fujian 350117, China
e-mail: cjwang1978@hit.edu.cn

Jian-Biao Wang
Institute of Materials Research and Engineering(IMRE), Agency for Science, Technology and Research (A*STAR), 2 Fusionopolis Way, Innovis #08-03, Singapore 138634, Republic of Singapore

Ming-Deng Wei
Fujian Provincial Key Laboratory of Electrochemical Energy Storage Materials, Fuzhou University, Fuzhou, Fujian, 350116, China

Zhen-Sheng Hong*
Academy of Carbon Neutrality of Fujian Normal University, Fuzhou, 350117, China

1 Introduction

Lithium-ion batteries (LIBs) have recently garnered great attention due to their cost-efficiency and high energy density [1-3] . It is expected that lithium metal batteries (LMBs) with Li metal as anode are promising candidate in realizing high energy density battery, owing to their high theoretical capacity (3860 mAh g^{-1}) and low standard electrode potential (3.04 V vs. SHE) [4-12] . However, conventional organic liquid electrolytes comprise flammable and volatile solvents, exhibiting instability and safety concerns. In contrast, Solid-state polymer electrolytes (SPEs) show enhanced thermal and electrochemical stability, and are therefore recognized as potential electrolyte candidates for next generation lithium batteries [13-15] .

Polymer electrolytes, particularly those based on polyethylene oxide (PEO) and polyvinylidene fluoride (PVDF) have the advantages of cost effectiveness, processing versatility, and excellent interfacial wettability. Nonetheless, their practical application are hindered by two significant challenges: the low ionic conductivity and the uneven lithium dendrite growth [16-21] . To address these issues, numerous strategies have been developed, including the incorporation of inorganic fillers [22-24] , the use of organic plasticizers [25-27] , the design of topology-enhanced polymers [28-30] , and the formation of stable interfaces [31-33] . Among these, inorganic fillers have been most extensively researched as they can enhance the mechanical strength and inhibit lithium dendrite formation. Common fillers include inert materials like Al_2O_3 [34, 35] , SiO_2 [36, 37] , and TiO_2 [38] , as well as active fillers [39-42] such as garnet-type $Li_7M_2Ln_3O_{12}$ (M=W, Te), NASICON-type $Li_{1.4}Al_{0.4}Ti_{1.6}(PO_4)_3$, perovskite-type $Li_7La_3Zr_2O_{12}$, and other ceramics [43, 44] . However, the weak interaction between inorganic fillers and the polymer matrix often reduces the filler efficacy, leading to poor lithium ion transport along the PEO-filler interface and unsatisfactory ionic conductivity. Furthermore, inorganic fillers simply act as physical barriers to prevent lithium dendrites from piercing the separator, without addressing the root cause.

A pioneering study by Liu et al [45] . demonstrated the use of composite SPEs containing metal-organic frameworks (MOFs) in all-solid-state lithium metal batteries

(ASSLMBs), yielding outstanding electrochemical performance and a stable electrolyte/electrode interface. Their findings revealed that unsaturated metal sites on the MOF surface function as Lewis acidic centers, preferentially anchoring anions of lithium salt and the polymer. This increases the lithium ion transference number (t_{Li+}) and enhances Li^+ mobility by promoting polymer segmental dynamics. These improvements are attributed to the MOFs' intrinsic porous structure, high surface area, periodic lattice, abundant Lewis acidic sites, and tunable functional groups. Consequently, various combinations of MOFs and metal salts to form MOF-based solid polymer electrolytes (MSPEs) have been studied to boost the ionic conductivity of solid-state electrolytes and suppress lithium dendrite growth [46-48] .

It is widely acknowledged that during charge/discharge, the migration of electrons between the cathode and anode prompts the movement of lithium salts, such as LiTFSI, within the electrolyte. In this process, anions ($TFSI^-$) migrate towards the anode, accumulating therein during lithium deposition, leading to uneven lithium deposition on the lithium metal surface and dendrite growth. Consequently, immobilizing anions within the electrolyte emerges as a promising strategy to mitigate lithium dendrite formation. Pioneering work by Liu et al. introduced the utilization of composite SPEs containing Metal-Organic Frameworks (MOFs) in ASSLMBs, yielding enhanced electrochemical performance and stable electrolyte/electrode interfaces. Their investigations elucidated that surface unsaturated metal sites serve as Lewis acidic centers, preferentially anchoring anions and polymers. This facilitates an increase in t_{Li+} through efficient anion absorption and enhances Li^+ mobility by promoting polymer segmental motion. These advancements are attributed to the intrinsic porous structure, high surface area, periodic crystal lattice, abundant Lewis acidic sites, and tunable functional groups inherent to MOFs.

MOF-74 constitutes a porous material with diverse metal clusters (Zn, Mn, Fe, Mg et al.), in conjunction with 2,5-dihydroxyterephthalic acid. This compound exhibits one-dimensional hexagonal channels and a dense array of open metal sites. In this work, the effect of Mg-MOF-74 (Mg-MOF) as an additive in SPE is presented. The exposed metal sites on Mg-MOF catalyze anion adsorption via Lewis acid-base interactions, thereby facilitating the dissociation of lithium salts. Consequently, this process reduces the crystallinity of the polymer matrix, thereby augmenting the amorphous domain. The ordered porous architecture of Mg-MOF ensures the uniform flux of lithium ions within the composite electrolyte, thus promoting homogeneous lithium deposition. The SPE@Mg-MOF has substantially enhanced ionic conductivity (5.2×10^{-4} S cm^{-1} at 60 ℃), commendable Li+ transference number (0.64), and an expanded electrochemical stability window (5.0 V). In Li//Li symmetric batteries, SPE@Mg-MOF effectively mitigates Li dendrite formation, attaining an extended cycle life exceeding 3000 hours with minimal voltage hysteresis. Notably, When SPE@Mg-MOF is utilized in a Li//$LiFePO_4$ full cell, it exhibits outstanding cycling stability, maintaining performance after 500 cycles at 60 ℃ and 1 C.

2 Experimental

Synthesis of Mg-MOF-74: 1.2 g of $(CH_3COO)_2Mg{\cdot}4H_2O$ (Aladdin) and 0.4 g of 2,5- dihydroxyterephthalic acid were dissolved into in a mixture of N, N-dimethylformamide, ethanol, and deionized water (12 mL: 4 mL: 4 mL). The mixture was subjected to ultrasonic treatment for 30 minutes to obtain a homogeneous solution, and then heated at 125 ℃ for 26 hours. After cooling, the resulting powder was washed three times with methanol, and dried in a vacuum oven at 60 ℃ for 24 hours.

Synthesis of SPEs: MOF-based polymer solid electrolytes were prepared using a solution casting method. First, polyethylene oxide (PEO, Mw=600, 000) and LiTFSI were dissolved in anhydrous acetonitrile with an [EO]/Li^+ molar ratio of 12. MOF fillers with different mass were then added to the solution. The mixture was mechanically stirred in dry air (humidity <40%) for 12 hours, followed by degassing under vacuum for 30 minutes. The solution was cast onto Teflon sheets and dried under vacuum at 65 ℃ for 12 hours to obtain the MOF-based polymer solid electrolytes. In this study, polymer solid electrolytes containing 0 wt%, 1 wt%, 5 wt%, and 10 wt% Mg-MOF are labeled as SPE, SPE@Mg-MOF-1, SPE@Mg-MOF, and SPE@Mg-MOF-10, respectively. The solid electrolytes containing 5 wt% of other MOFs (Bi-MOF and Co-MOF) are named as SPE@Bi-MOF and SPE@Co-MOF.

3 Results and discussion

Mg-MOF synthesized via hydrothermal methods comprises Mg^{2+} metal ion nodes and 2,5-dihydroxyterephthalic acid organic ligands. Fig. 1a shows the preparation process of SPE@Mg-MOF (synthetic method detailed in the Supporting Information). Scanning electron microscopy (SEM) (Fig. 1b) reveals Mg-MOF particles with a size of approximately 1 μm, and a uniform morphology ideal for polymer solid electrolyte preparation. The cross-sectional SEM image of SPE@Mg-MOF (Fig. 1c) exhibits an even thickness of about 70 μm, with energy dispersive spectroscopy (EDS) showing the uniform distribution of Mg, N, F, and S elements. While pure SPE surfaces have cracks and pores, SPE@Mg-MOF surfaces appear smoother. This is attributed to the hydroxyl groups of Mg-MOF, capable of forming hydrogen bonds with ether oxygen bonds and terminal hydroxyl groups on the PEO segment, while the steric hindrance of Mg-MOF groups prevents agglomeration. With increasing Mg-MOF content, agglomeration on the SPE substrate increases, leading to cracks on the surface of SPE@Mg-MOF-10 (Figs. S1, S2). Moreover, EDS analysis (Fig. 1g) further validates the effective dispersion of Mg-MOF in the polymer solid electrolyte substrate.

The phase structures of Mg-MOF, SPE, SPE@Mg-MOF-1, SPE@Mg-MOF, and SPE@Mg-MOF-10 electrolytes were investigated using X-ray diffraction (XRD), as illustrated in Fig. 2a. The intensities of several characteristic peaks of Mg-MOF increase as a result of changes in mass fraction. Notably, compared to SPE, the characteristic peaks of PEO and Mg-MOF in SPE@Mg-MOF-1, SPE@Mg-MOF, and SPE@Mg-MOF-10 electrolytes are distinctly observable, indicating a good mixing between additives and the polymer substrate. Strong intermolecular interactions were examined in detail using atomic force microscopy (AFM) to assess their influence on surface micromorphology. Figs. 2b, S3 reveal that PEO-LiTFSI exhibits a heterogeneous morphology characterized by severe particle aggregation and surface cracks. In contrast, SPE@Mg-MOF (Figs. 2c, S3) displays a smooth surface with a significant reduction in the size of the PEO crystal region, facilitating the construction of a continuous ion diffusion pathway.

Fourier transform infrared (FT-IR) spectroscopy was employed to examine the coordination environment of SPE@Mg-MOF. As illustrated in Fig. 2d, the asymmetric sum of $-CF_3$ in LiTFSI is evident at 1182 cm^{-1} and 1215 cm^{-1}, accompanied by symmetrical stretching vibration peaks and the bending vibration peak of $-CF_3$ at 840 cm^{-1}. Upon introducing 5% Mg-MOF into the PEO matrix, the characteristic peak of $-CF_3$ exhibits a notable weakening. With a subsequent increase in the Mg-MOF content, the intensity of this characteristic peak gradually increases. This observation suggests that at lower concentrations, Mg-MOF disperses readily within the PEO matrix, serving as a Lewis acidic center to adsorb $TFSI^-$, thereby facilitating the dissociation of LiTFSI. However, at higher Mg-MOF concentrations, agglomeration occurs within the PEO matrix, leading to reduced $TFSI^-$ adsorption on the Mg-MOF surface and consequently, an increase in peak intensity [49] .

Further analysis using Raman spectroscopy were conducted to investigate the alterations in the chemical milieu encompassing lithium ions within SPE@Mg-MOF. As shown in Fig. 2e, Gaussian-Lorentz fitting of the Raman spectra delineates wavelengths at 736−740 cm^{-1} as "free uncoordinated $TFSI^-$" and at 744−747 cm^{-1} as "$TFSI^-$ coordinated with Li^+". The ratio of free lithium salt anions was calculated using the following equation:

$$[free\ TFSI^-] = \frac{A(free)}{A(free) + A(TFSI^-\ coordinated\ with\ Li^+)} \times 100\%$$

By integrating filler materials endowed with Lewis acid properties and fostering Lewis acid-base interactions between the filler and LiTFSI, we observed that the dissociation degree of SPE@Mg-MOF surged to 903%, surpassing the 71.7% dissociation observed in LiTFSI within the PEO electrolyte (Fig. S4).

The homogeneous dispersion of Mg-MOF within the SPE provides robust mechanical reinforcement, crucial for mitigating lithium dendrite formation. The mechanical properties of the resulting polymer electrolyte were assessed via stress-strain curves, depicted in Fig. 2f and g. Notably, the fracture elongation of the SPE@Mg-MOF membrane reaches 1500%, significantly surpassing that of the SPE (500%). These curves can be classified to three distinct regions: pre-necking, necking, and strain hardening. In the pre-necking phase, stress escalates rapidly with strain in both SPE variants, attributable to alterations in polymer bond length and angle, facilitating reversible elastic behavior. Subsequently, in the necking phase, stress stabilizes as strain increases, primarily due to polymer chain mobility. Transitioning to the strain hardening phase, stress rises linearly with strain, accompanied by polymer chain alignment in the stretching direction. The heightened mechanical resilience is ascribed to the interaction between the active surface of Mg-MOF and PEO chains, culminating in the formation of physical cross-links. Under external mechanical loads, Mg-MOF acts as pivotal cross-linking points, effectively dispersing stress and redistributing it across other polymer chains,thereby impeding the growth of lithium dendrites.

Thermal stability assessment of the electrolyte was conducted using thermogravimetric analysis (TGA). As depicted in Fig. 2h, within the temperature range of 300 ℃ to 400 ℃, approximately 80% weight loss was observed for SPE, SPE@Mg-MOF-1, SPE@Mg-MOF, and SPE@Mg-MOF-10, primarily attributed to the decomposition of PEO and LiTFSI. Upon further heating to 600 ℃, the residual amounts for SPE@Mg-MOF-1, SPE@Mg-MOF, and SPE@Mg-MOF-10 were approximately 3.5 wt%, 6.0 wt%, and 11.0 wt%, respectively, correlating with the additive mass. In contrast, the SPE began decomposing around 200 ℃, with a final residual mass of approximately 2.5 wt%. These results underscore the improved thermal stability induced by the inclusion of Mg-MOF in the SPE matrix.

The electrochemical stability window at 60 ℃ was assessed using linear sweep voltammetry (LSV) measurements, with the results depicted in Fig. 3a. Compared to SS/SPE/Li, SS/SPE@Mg-MOF/Li exhibited a broader electrochemical window (5.0 V), rendering it compatible with most cathode materials. Li/SPE@Mg-MOF/Li symmetric cell was employed to assess the mobility of Li^+ ions within the electrolyte. A high lithium ion transference number is advantageous for minimizing polarization and suppressing side reactions. Conversely, a low lithium ion transference number represents a fundamental drawback of traditional lithium battery electrolytes, as an excess of mobile anions can elevate electrode polarization and spur interface side reactions [50] . As illustrated in Fig. 3b, DC polarization testing revealed a t_{Li+} of 0.64 for SPE@Mg-MOF. This elevated t_{Li+} can be ascribed to the interaction between the abundant active sites on the surface of Mg-MOF and TFSI-, effectively impeding anion movement and augmenting Li^+ migration. Moreover, electronic conductivities for SPE, SPE@Mg-MOF-1, SPE@Mg-MOF, and SPE@Mg-MOF-10 were measured to be 1.7×10^{-4}, 1.9×10^{-4}, 5.2×10^{-4} and 2.31×10^{-4} S cm^{-1}, respectively (Fig. S5, S6). The introduction of Mg-MOF into PEO-based electrolytes widens the electrochemical operating window, enhances ionic conductivity, and elevates the Li^+ migration number, collectively improving the performance of solid-state lithium metal batteries.

Furthermore, we also conducted a comparative analysis involving classic MOFs (ZIF67, Bi-BTC) from different series in this study (Figs. S7-S11). Remarkably, under equivalent addition amounts, SPE@Mg-MOF exhibited superior ionic conductivity (Fig. 3c). Additionally, we assessed the proportion of free lithium salt anions via Raman spectroscopy and FT-IR absorption spectroscopy (Figs. S12, S13), with SPE@Bi-MOF demonstrating a dissociation degree of 77% and SPE@Co-MOF of 83%. As depicted in Fig. 3d, S14, symmetrical cells assembled using SPE@Mg-MOF delivered stable Li plating/stripping over 3000 hours at current densities of 0.1 mA cm^{-2} and 0.1 mAh cm^{-2}, with an overpotential of merely 35 mV. This exceptional performance is attributed to the outstanding mechanical properties, rapid ion transmission, and uniform lithium ion flux facilitated by SPE@Mg-MOF, surpassing that of SPE@Bi-MOF and SPE@Co-MOF.

Fig. 4a–c displays SEM images of the lithium surface before and after cycling with SPE, and after 50 cycles, respectively. In the SPE-assembled battery, the lithium surface exhibits uneven dendrite deposition, forming island-shaped "dead lithium." Conversely, the surface of the SPE@Mg-MOF remains smooth and flat, indicating a uniform lithium deposition. To elucidate the mechanism underlying the excellent electrochemical performance, the stability of the interface between the electrolyte and electrode was investigated. XPS analysis of SPE@Mg-MOF before and after Li//Li symmetric battery cycling was conducted to determine the composition of its solid electrolyte interphase (SEI) film. The C1s spectrum (Fig. 4d) reveals signals corresponding to five components: C-C, -COR, -COOR, -CF2, and -CF_3, at 284.8 eV, 286.4 eV, 287.8 eV, 289.6 eV, and 292.7 eV, respectively, indicating the coexistence of organic and inorganic compounds in the SEI layer [51] . The appearance of -CF_2 after etching suggests the dissociation of -CF_3. Additionally, the binding energies of the F1s spectra at 684.8 eV and 688.7 eV correspond to LiF and C-F (including -CF_2, -CF_3), respectively, as shown in Fig. 4e. The F1s spectrum of C-F originates from TFSI-, while LiF constitutes the main inorganic component of the SEI. Moreover, the XPS spectrum reveals the signals of Li_2CO_3, LiS, and Li_2O on the contact side with SPE@Mg-MOF (Fig. 4f), which are common passivation products of Li anodes. The formation of a stable interface with a lithium-rich SEI is conducive to inhibiting the growth of lithium dendrites in Li/SPE@Mg-MOF/Li batteries.

To verify the practical feasibility of SPE@Mg-MOF, Li/SPE@Mg-MOF/$LiFePO_4$ full-cells (Fig. 5a) were assembled and assessed. As shown in Figs. 5b, S15, the LFP/SPE@Mg-MOF/Li battery delivers discharge capacities of 169.4, 168.9, 168.3, 167.9, 163.3, and 145.7 mAh g^{-1} at rates of 0.1 C, 0.2 C, 0.5 C, 1 C, 2 C, and 5 C, respectively. It exhibits notable capacity retention upon reverting to a 0.5 C discharge rate. In contrast, the LFP/SPE/Li batteries exhibit inferior rate performance, yielding discharge capacities of 134.5, 132.3, 123.7, 87.1, 46.7, and 21 mAh g^{-1}, respectively, at rates of 0.1 C, 0.2 C, 0.5 C, 1 C, 2 C, and 5 C. The charge-discharge curves in Fig. 5c demonstrate a consistent voltage plateau for the LFP/SPE@Mg-MOF/Li battery, indicative of minimal polarization effects. Furthermore, the LFP/SPE@Mg-MOF/Li battery exhibits robust cycle stability, retaining 80% of its capacity even after 500 cycles at 1 C. Notably, the electrolyte has shown substantial improvements in ionic conductivity, transference number and cycling stability compared to recently reported literatures (Table S1, S2).

4 Conclusion

In this work, we successfully prepared Mg-MOF modified PEO-based SPE with outstanding mechanical properties and high ionic conductivity. The Mg-MOF modified SPE exhibits excellent mechanical performance, effectively inhibiting the growth of lithium dendrites. The polar functional groups on the organic ligands in Mg-MOF interacted with the PEO chains greatly enhance the Li^+ transport. Compared to the Bi-MOF and Co-MOF, Mg-MOF shows a stronger adsorption capacity for $TFSI^-$. Consequently, SPE@MgMOF demonstrates high ionic conductivity and a wide electrochemical stability window (1.0-5.0 V). As a result, it exhibits an ultra-long cycle life of over 3000 hours in lithium symmetric cells. Furthermore, a full cell paired with LFP cathode displays a excellent rate capability and cycling performance. This study firstly demonstrates a new MOF material introduced in PEO-based ASSLMBs with outstanding cycling and rate performance.

Acknowledgments This work was financially supported by National Natural Science Foundation of China (NSFC 52374302 and 51874099) and Natural Science Foundation of Fujian Province's Key Project (2021J02031). Z. H. also thanks the support from the open fund from Academy of Carbon Neutrality of Fujian Normal University (TZH2022-06). We also thank the Undergraduate Training Programs for Innovation and Entrepreneurship (cxx1-2024363)

Declarations

Conflict of interests The authors declare that they have no conflict of interest.

References

[1] Li M, Lu J, Chen Z, Amine K. 30 years of lithium-ion batteries. Adv Mater. 2018. https://doi.org/10.1002/adma.201800561.

[2] Winter M, Barnett B, Xu K. Before li ion batteries. Chem Rev. 2018;118. https://doi.org/10.1021/acs.chemrev.8b00422.

[3] Gao Y-M, Liu Y, Feng K-J, Ma J-Q, Miao Y-J, Xu B-R, Pan K-M, Akiyoshi O, Wang GX, Zhang KK, Zhang Q-B. Emerging ws2/wse2@graphene nanocomposites: Synthesis and electrochemical energy storage applications. Rare Met. 2023;43:1. https://doi.org/10.1007/s12598-023-02424-8.

[4] Lu G, Nai J, Luan D, Tao X, Lou XWD. Surface engineering toward stable lithium metal anodes. Sci Adv. 2023;9. https://doi.org/10.1126/sciadv.adf1550.

[5] Kang J, Han DY, Kim S, Ryu J, Park S. Multiscale polymeric materials for advanced lithium battery applications. Adv Mater. 2023;35. https://doi.org/10.1002/adma.202203194.

[6] Liu Y, Tao X, Wang Y, Jiang C, Ma C, Sheng O, Lu G, Lou XWD. Self-assembled monolayers direct a lif-rich interphase toward long-life lithium metal batteries. Science. 2022;375.

https://doi.org/10.1126/science.abn1818.
[7] Fan L-Z, He H, Nan C-W. Tailoring inorganic–polymer composites for the mass production of solid-state batteries. Nat Rev Mater. 2021;6:1003. https://doi.org/10.1038/s41578-021-00320-0.
[8] Ye C, Shan J, Li H, Kao CC, Gu Q, Qiao SZ. Reducing overpotential of solid-state sulfide conversion in potassium-sulfur batteries. Angew Chem Int Ed. 2023;62. https://doi.org/10.1002/anie.202301681.
[9] Zhang R, Li NW, Cheng XB, Yin YX, Zhang Q, Guo YG. Advanced micro/nanostructures for lithium metal anodes. Adv Sci. 2017;4. https://doi.org/10.1002/advs.201600445.
[10] Gong Y, Wang C, Xin M, Chen S, Xu P, Li D, Liu J, Wang Y, Xie H, Sun X, Liu Y. Ultra-thin and high-voltage-stable bi-phasic solid polymer electrolytes for high-energy-density li metal batteries. Nano Energy. 2024;119:109054. https://doi.org/10.1016/j.nanoen.2023.109054.
[11] Liao JL, Zhang S, Bai TS, Ji FJ, Li DP, Cheng J, Zhang H-Q, Lu J-Y, Gao Q, Ci L-J. A zno decorated 3d copper foam as a lithiophilic host to construct composite lithium metal anodes for li–o2 batteries. Rare Met. 2023;42:1969. https://doi.org/10.1007/s12598-023-02281-5.
[12] Zhang S, Xiao S, Li D, Liao J, Ji F, Liu H, Ci L. Commercial carbon cloth: An emerging substrate for practical lithium metal batteries. Energy Storage Mater. 2022;48:172. https://doi.org/10.1016/j.ensm.2022.03.014.
[13] Wu F, Tan G, Chen R, Li L, Xiang J, Zheng Y. Novel solid-state li/lifepo(4) battery configuration with a ternary nanocomposite electrolyte for practical applications. Adv Mater. 2011;23. https://doi.org/10.1002/adma.201103161.
[14] Choudhury S, Mangal R, Agrawal A, Archer LA. A highly reversible room-temperature lithium metal battery based on crosslinked hairy nanoparticles. Nat Commun. 2015;6. https://doi.org/10.1038/ncomms10101.
[15] Liu Z, Liu P, Tian L, Xiao J, Cui R, Liu Z. Significantly enhancing the lithium-ion conductivity of solid-state electrolytes via a strategy for fabricating hollow metal-organic frameworks. Chem Commun. 2020;56. https://doi.org/10.1039/d0cc06022d.
[16] Li Z, Huang J, Yann Liaw B, Metzler V, Zhang J. A review of lithium deposition in lithium-ion and lithium metal secondary batteries. J Power Sources. 2014;254:168. https://doi.org/10.1016/j.jpowsour.2013.12.099.
[17] Zhang Q, Liu K, Ding F, Liu X. Recent advances in solid polymer electrolytes for lithium batteries. Nano Res. 2017;10:4139. https://doi.org/10.1007/s12274-017-1763-4.
[18] Meyer WH. Polymer electrolytes for lithium-ion batteries. Adv Mater. 1998;10:439. https://doi.org/10.1002/(sici)1521-4095(199804)10:6<439::Aid-adma439>3.0.Co;2-i.
[19] Fang R, Xu H, Xu B, Li X, Li Y, Goodenough JB. Reaction mechanism optimization of solid state li s batteries with a peo based electrolyte. Adv Funct Mater. 2020;31. https://doi.org/10.1002/adfm.202001812.
[20] Ma Y, Zhang R, Wang L, Wu J, Chen B, Yu Y, Li L, He F, Shi C, Zhao N, He C, Wong AB. Self-healing polymer-based electrolyte induced by amorphous three-dimensional carbon for high-performance solid-state li metal batteries. Energy Storage Mater. 2023;61:102893. https://doi.org/10.1016/j.ensm.2023.102893.
[21] Chen S, Ma S, Liu Z, Li Y, Yin H, Song H, Zhang M, Xin M, Sun L, Liu Y, Xie H, Cong L. Structurally integrated asymmetric polymer electrolyte with stable janus interface properties for high-voltage lithium metal batteries. J Colloid Interface Sci. 2023;638. https://doi.org/10.1016/j.jcis.2023.01.125.
[22] Tao J, Chen Y, Bhardwaj A, Wen L, Li J, Kolosov OV, Lin Y, Hong Z, Huang Z, Mathur S. Combating li metal deposits in all-solid-state battery via the piezoelectric and ferroelectric effects. Proc Natl Acad Sci. 2022;119. https://doi.org/10.1073/pnas.2211059119.
[23] Liu Y, Wang P, Yang Z, Wang L, Li Z, Liu C, Liu B, Sun Z, Pei H, Lv Z, Hu W, Lu Y, Zhu G. Lignin derived ultrathin all-solid polymer electrolytes with 3d single-ion nanofiber ionic bridge framework for high performance lithium batteries. Adv Mater. 2024. https://doi.org/10.1002/adma.202400970.
[24] Li L, Duan H, Li J, Zhang L, Deng Y, Chen G. Toward high performance all‐solid‐state lithium batteries with high‐voltage cathode materials: Design strategies for solid electrolytes, cathode interfaces, and composite electrodes. Adv Energy Mater. 2021;11. https://doi.org/10.1002/aenm.202003154.
[25] Kim E, Jamal H, Jeon I, Khan F, Chun SE, Kim JH. Functionality of 1 butyl 2,3 dimethylimidazolium bromide (bmi‐br) as a solid plasticizer in peo‐based polymer electrolyte for highly reliable lithium metal batteries. Adv Energy Mater. 2023;13. https://doi.org/10.1002/aenm.202301674.
[26] Bao W, Zhang Y, Cao L, Jiang Y, Zhang H, Zhang N, Liu Y, Yan P, Wang X, Liu Y, Li H, Zhao Y, Xie J. An h2o‐initiated crosslinking strategy for ultrafine‐nanoclusters‐reinforced high‐toughness polymer‐in‐plasticizer solid electrolyte. Adv Mater. 2023;35. https://doi.org/10.1002/adma.202304712.
[27] Zhang J, Chou J, Luo XX, Yang YM, Yan MY, Jia D, Zhang CH, Wang YH, Wang WP, Tan SJ, Guo JC, Zhao Y, Wang F, Xin S, Wan LJ, Guo YG. A fully amorphous, dynamic cross-linked polymer electrolyte for lithium-sulfur batteries operating at subzero-temperatures. Angew Chem Int Ed. 2024;63. https://doi.org/10.1002/anie.202316087.
[28] Li Y, Zhang J, Chen Q, Xia X, Chen M. Emerging of heterostructure materials in energy storage: A review. Adv Mater. 2021;33. https://doi.org/10.1002/adma.202100855.
[29] Liu Y, Zeng Q, Li Z, Chen A, Guan J, Wang H, Wang S, Zhang L. Recent development in topological polymer electrolytes for rechargeable lithium batteries. Adv Sci. 2023;10. https://doi.org/10.1002/advs.202206978.
[30] Anderson CL, Li H, Jones CG, Teat SJ, Settineri NS, Dailing EA, Liang J, Mao H, Yang C, Klivansky LM, Li X, Reimer JA, Nelson HM, Liu Y. Solution-processable and functionalizable ultra-high molecular weight polymers via topochemical synthesis. Nat Commun. 2021;12. https://doi.org/10.1038/s41467-021-27090-1.
[31] Meng N, Ye Y, Yang Z, Li H, Lian F. Developing single‐ion conductive polymer electrolytes for high‐energy‐density solid state batteries. Adv Funct Mater. 2023;33. https://doi.org/10.1002/adfm.202305072.
[32] Pei F, Wu L, Zhang Y, Liao Y, Kang Q, Han Y, Zhang H, Shen Y, Xu H, Li Z, Huang Y. Interfacial self-healing polymer electrolytes for long-cycle solid-state lithium-sulfur batteries. Nat Commun. 2024;15. https://doi.org/10.1038/s41467-023-43467-w.
[33] Liu Y, Feng K, Han J, Wang F, Xing Y, Tao F, Li H, Xu B, Ji J, Li H. Regulation of Zn^{2+} solvation shell by a novel n-methylacetamide based eutectic electrolyte toward high-performance zinc-ion batteries. Journal of Materials Science & Technology. 2025;211:53. https://doi.org/10.1016/j.jmst.2024.05.030.
[34] Wang J, Fan L, Du Q, Jiao K. Lithium ion transport in solid polymer electrolyte filled with alumina nanoparticles. Energy Adv. 2022;1:269. https://doi.org/10.1039/d2ya00025c.
[35] He Y, Zhang Y, Wang Z, Li X, Lü Z, Huang X, Liu Z. In situ surface film formed by solid‐state anodic oxidation for stable lithium metal anodes. Adv Funct Mater. 2021;31. https://doi.org/10.1002/adfm.202101737.
[36] Zhao Y, Li L, Zhou D, Ma Y, Zhang Y, Yang H, Fan S, Tong H, Li S, Qu W. Opening and constructing stable lithium-ion channels within polymer electrolytes. Angew Chem Int Ed. 2024. https://doi.org/10.1002/anie.202404728.
[37] Wang H, Wang F, Liu Y, Liu Z, Miao Y, Zhang W, Wang G, Ji J,

Zhang Q. Emerging natural clay-based materials for stable and dendrite-free lithium metal anodes: A review. Chin Chem Lett. 2024109589. https://doi.org/10.1016/j.cclet.2024.109589.
[38] Li J, Cai Y, Zhang F, Cui Y, Fang W, Da H, Zhang H, Zhang S. Exceptional interfacial conduction and lif interphase for ultralong life peo-based all-solid-state batteries. Nano Energy. 2023;118:108985. https://doi.org/10.1016/j.nanoen.2023.108985.
[39] Qian S, Zhu H, Sun C, Li M, Zheng M, Wu Z, Liang Y, Yang C, Zhang S, Lu J. Liquid metal loaded molecular sieve: Specialized lithium dendrite blocking filler for polymeric solid-state electrolyte. Adv Mater. 2024. https://doi.org/10.1002/adma.202313456.
[40] Fang C, Huang K, Zhao J, Tian S, Dou H, Zhang X. Dual-filler reinforced pvdf-hfp based polymer electrolyte enabling high-safety design of lithium metal batteries. Nano Res. 2024;17:5251. https://doi.org/10.1007/s12274-024-6502-z.
[41] Liu YN, Xiao Z, Zhang WK, Zhang J, Huang H, Gan YP, He XP, Kumar GG, Xia Y. Poly(m-phenylene isophthalamide)-reinforced polyethylene oxide composite electrolyte with high mechanical strength and thermostability for all-solid-state lithium metal batteries. Rare Met. 2022;41:3762. https://doi.org/10.1007/s12598-022-02065-3.
[42] Liang Y, Wu W, Li D, Wu H, Gao C, Chen Z, Ci L, Zhang J. Highly stable lithium metal batteries by regulating the lithium nitrate chemistry with a modified eutectic electrolyte. Adv Energy Mater. 2022;12. https://doi.org/10.1002/aenm.202202493.
[43] Liu S, Liu W, Ba D, Zhao Y, Ye Y, Li Y, Liu J. Filler-integrated composite polymer electrolyte for solid-state lithium batteries. Adv Mater. 2023;35. https://doi.org/10.1002/adma.202110423.
[44] Chen H, Huang ZY, Chen SL, Tong RA, Wang HL, Shao G, Wang CA. In situ polymerization of 1,3-dioxolane infiltrating 3d garnet framework with high ionic conductivity and excellent interfacial stability for integrated solid-state li metal battery. Rare Met. 2022;41:3694. https://doi.org/10.1007/s12598-022-02080-4.
[45] Yuan C, Li J, Han P, Lai Y, Zhang Z, Liu J. Enhanced electrochemical performance of poly(ethylene oxide) based composite polymer electrolyte by incorporation of nano-sized metal-organic framework. J Power Sources. 2013;240:653. https://doi.org/10.1016/j.jpowsour.2013.05.030.
[46] Yuan S, Bao JL, Wei J, Xia Y, Truhlar DG, Wang Y. A versatile single-ion electrolyte with a grotthuss-like li conduction mechanism for dendrite-free li metal batteries. Energy Environ Sci. 2019;12:2741. https://doi.org/10.1039/c9ee01473j.
[47] Zhou X, Zhang B, Huang F, Li F, Ma Z, Liu J. Difunctional mof for dendrite-free all-solid-state lithium metal batteries by synergistic effect of hydrogen bond and electrostatic interaction. Nano Energy. 2023;108:108221. https://doi.org/10.1016/j.nanoen.2023.108221.
[48] Dong P, Zhang X, Hiscox W, Liu J, Zamora J, Li X, Su M, Zhang Q, Guo X, McCloy J, Song MK. Toward high-performance metal-organic-framework-based quasi-solid-state electrolytes: Tunable structures and electrochemical properties. Adv Mater. 2023;35. https://doi.org/10.1002/adma.202211841.
[49] Mathew DE, Gopi S, Kathiresan M, Stephan AM, Thomas S. Influence of mof ligands on the electrochemical and interfacial properties of peo-based electrolytes for all-solid- state lithium batteries. Electrochim Acta. 2019;319:189. https://doi.org/10.1016/j.electacta.2019.06.157.
[50] Zhou P, Zhang X, Xiang Y, Liu K. Strategies to enhance li+ transference number in liquid electrolytes for better lithium batteries. Nano Res. 2022;16:8055. https://doi.org/10.1007/s12274-022-4833-1.
[51] Yao M, Yu T, Ruan Q, Chen Q, Zhang H, Zhang S. High-voltage and wide-temperature lithium metal batteries enabled by ultrathin mof-derived solid polymer electrolytes with modulated ion transport. ACS Appl Mater Interfaces. 2021;13. https://doi.org/10.1021/acsami.1c15038.

标题:Mg-MOF 基稳定的无枝晶金属锂固态电池

作者名：陈旭东，赵思，冯鑫福 黄锦 王妍 邱圳春 王建标 黄艺吟 魏明灯 郑力拓 洪振生
作者单位：福建师范大学物理与能源学院

摘要 (Chinese Abstract)：固态聚合物电解质（SPE）的广泛应用受限于其有限的离子导电性、窄电化学窗口以及锂枝晶问题。在本研究中，我们将 Mg-MOF 引入聚氧化乙烯（PEO）基聚合物固态电解质中，导致电解质界面原位生成 LiF 及其他化合物。这一改性显著提升了锂离子的传输能力，并有效调控了锂沉积行为，从而抑制了锂枝晶的形成。Mg-MOF 作为路易斯酸位点，有助于阴离子吸附并促进 LiTFSI 的解离，同时提供额外的位点用于锂离子的络合/解络合。实验结果显示，在 0.1 mA cm^{-2} 的电流密度下，对称 Li//Li 电池表现出 35 mV 的低过电位，并在超过 3000 小时的循环中实现了稳定的镀锂/剥锂性能。SPE@Mg-MOF 在 60℃下的离子导电性达到 5.2 × 10^{-4} S cm^{-1}，锂离子迁移数为 0.64。因此，Li/SPE@Mg-MOF/$LiFePO_4$ 全电池在 0.1 C 倍率下的放电容量为 169.4 mAh g^{-1}，在 5 C 倍率下的容量为 145.7 mAh g^{-1}，且在 1 C 倍率下稳定循环 500 次后仍保持 80%的容量保持率。

Figures

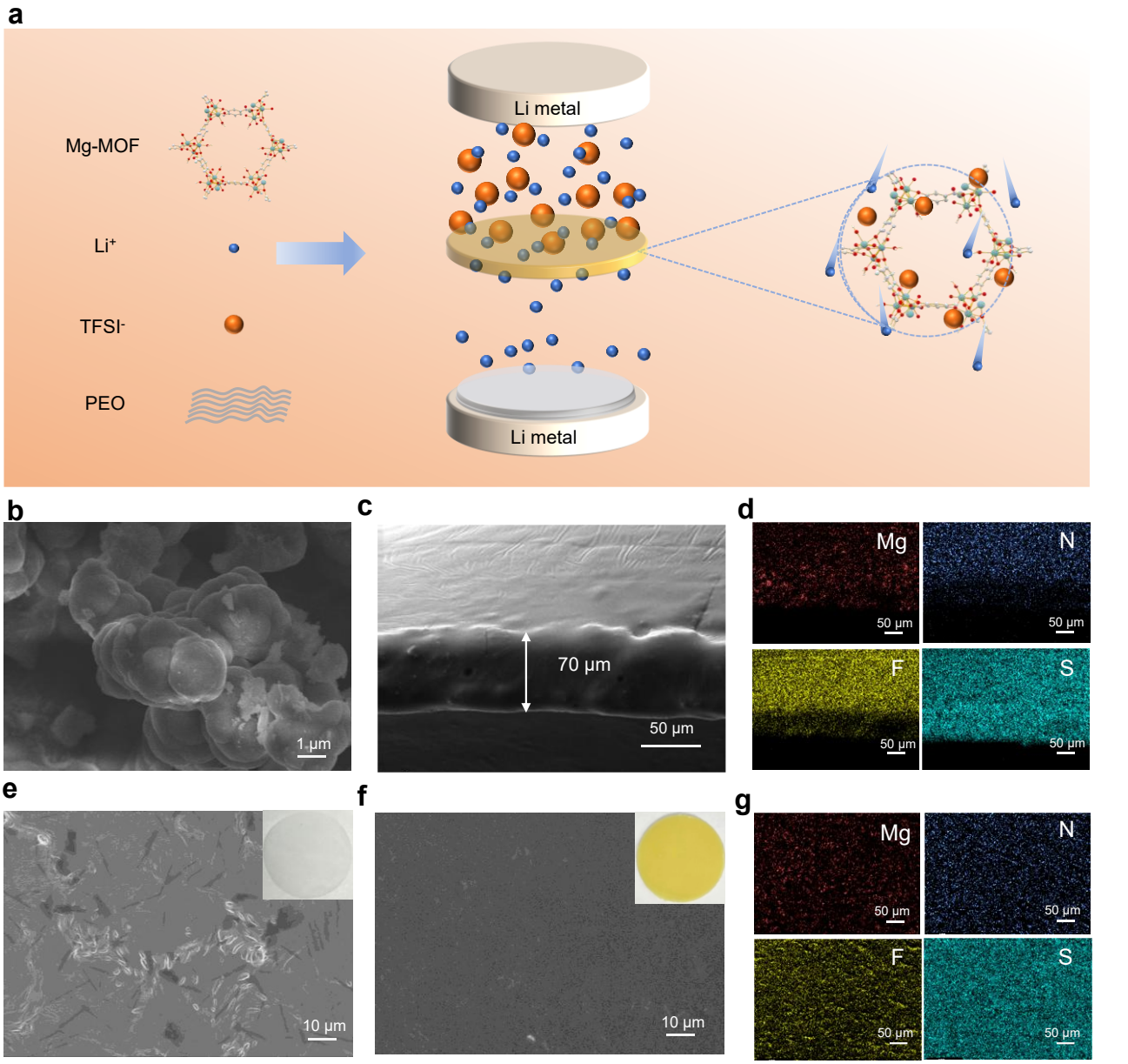

Fig. 1 **a** Schematic illustration of the synthetic route of SPE@Mg-MOF electrolytes; **b** SEM images of Mg-MOF; **c** Cross-sectional SEM image of SPE@Mg-MOF; **d** EDS mapping obtained from Fig. 1c, **e** SEM images of SPE; **f** SEM images of SPE@Mg-MOF; **g** EDS mapping obtained from Fig. 1f.

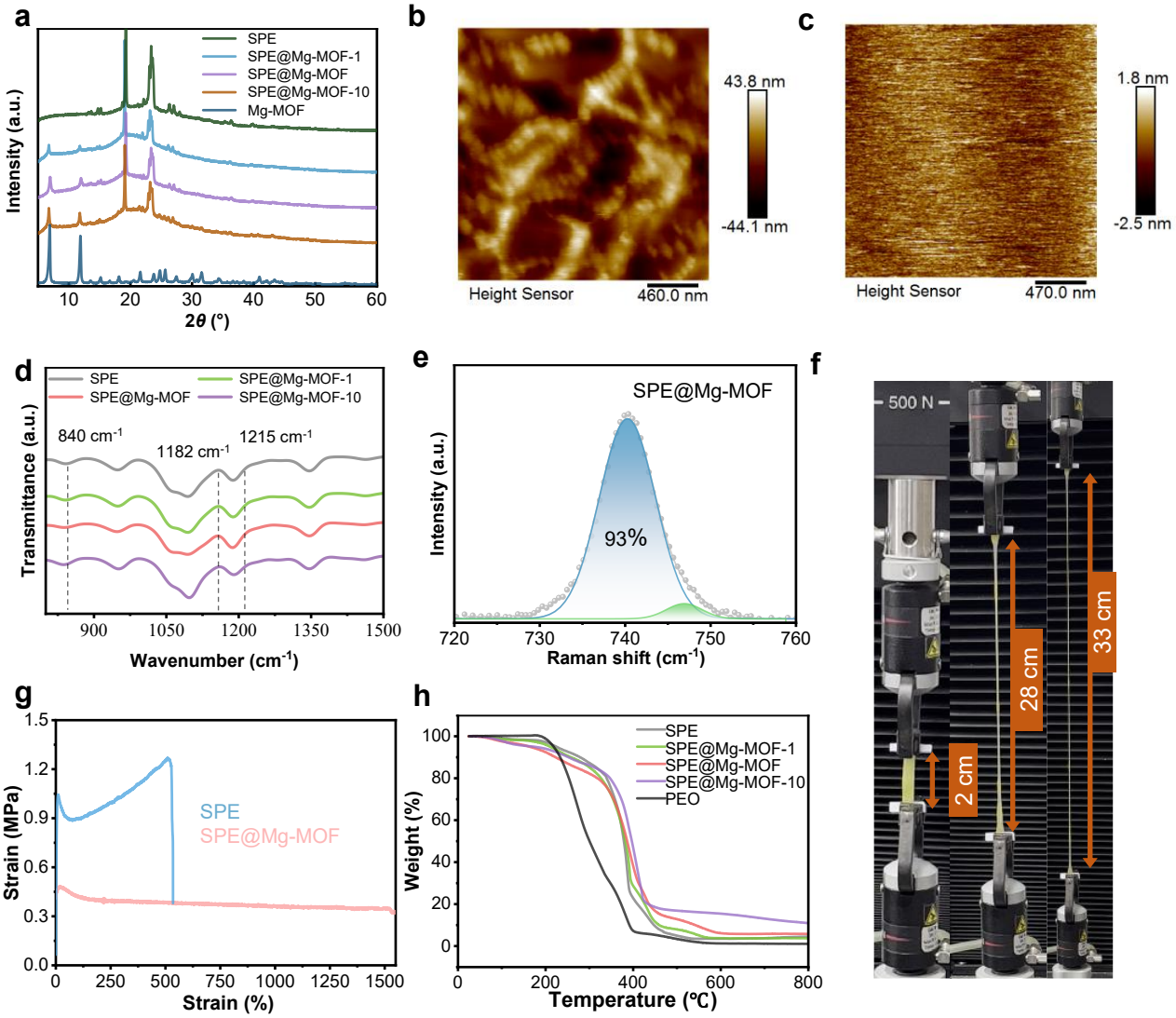

Fig. 2 **a** XRD patterns of SPE, Mg-MOF, and SPE@Mg-MOF. **b** AFM of SPE@Mg-MOF. **c** AFM of SPE. **d** FT-IR spectrum of SPE, and SPE@Mg-MOF. **e** Raman spectrum of SPE@Mg-MOF. **f** Optical image of the SPE@Mg-MOF membrane during stress-strain measurement. **g** Stress-strain curves of PEO-based electrolyte. **h** TGA curves.

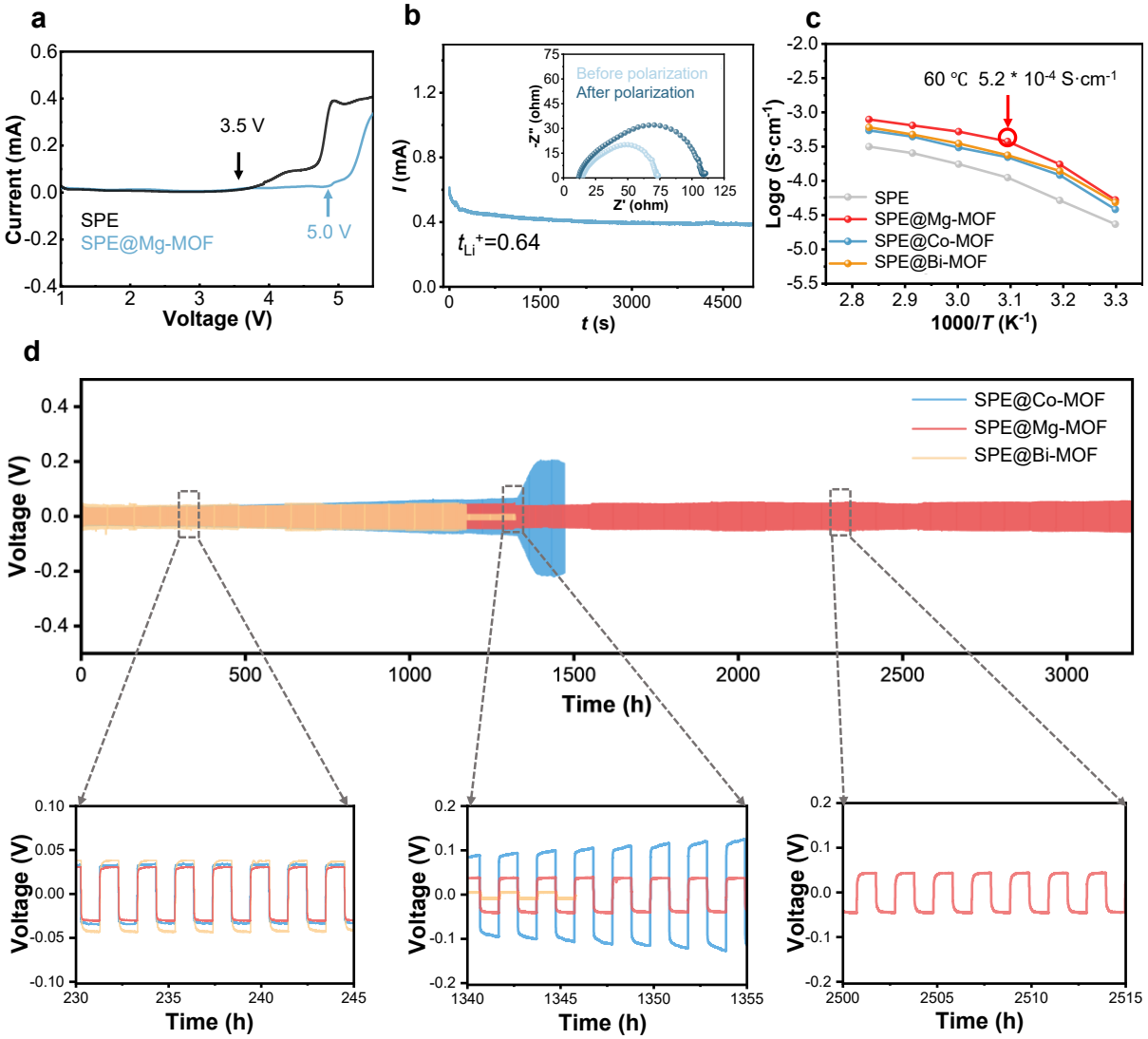

Fig. 3 **a** LSV curves of SPE and SPE@Mg-MOF. **b** Li/SPE@Mg-MOF/Li cells after a perturbation of 10 mV direct current pulse. Inset: impedance spectra of the cells before and after the dc polarization at 60 ℃. **c** Arrhenius plots of ionic conductivity. **d** Charge/discharge voltage curves of Li/SPE@Mg-MOF/Li, Li/SPE@Co-MOF/Li and Li/SPE@Bi-MOF/Li cells at 60 ℃ with 0.1 mA cm^{-2}.

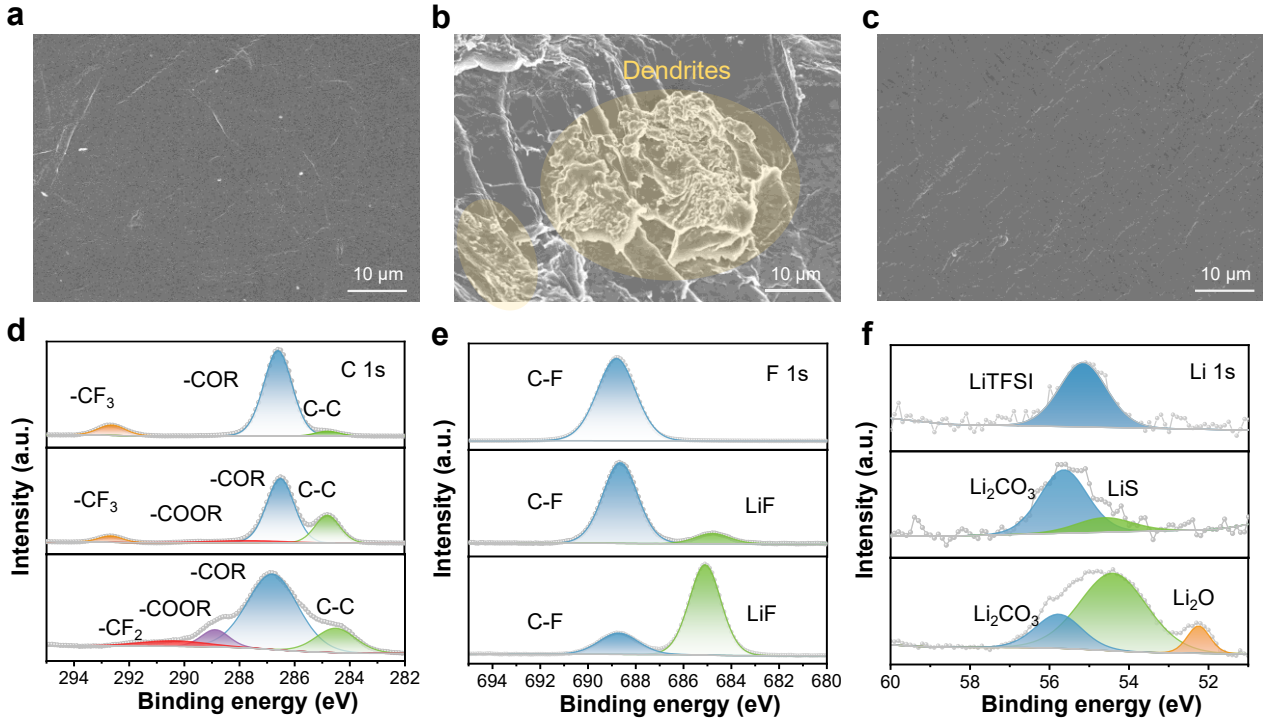

Fig. 4 **a** The SEM of Li anode before cycling. **b** The SEM of Li anode after 50 cycles for Li/SPE/Li. **c** The SEM of Li anode after 50 cycles for Li/SPE@Mg-MOF/Li. XPS on SPE@Mg-MOF surface before and after 50 cycles: **d** C 1s, **e** F 1s, and **f** Li 1s.

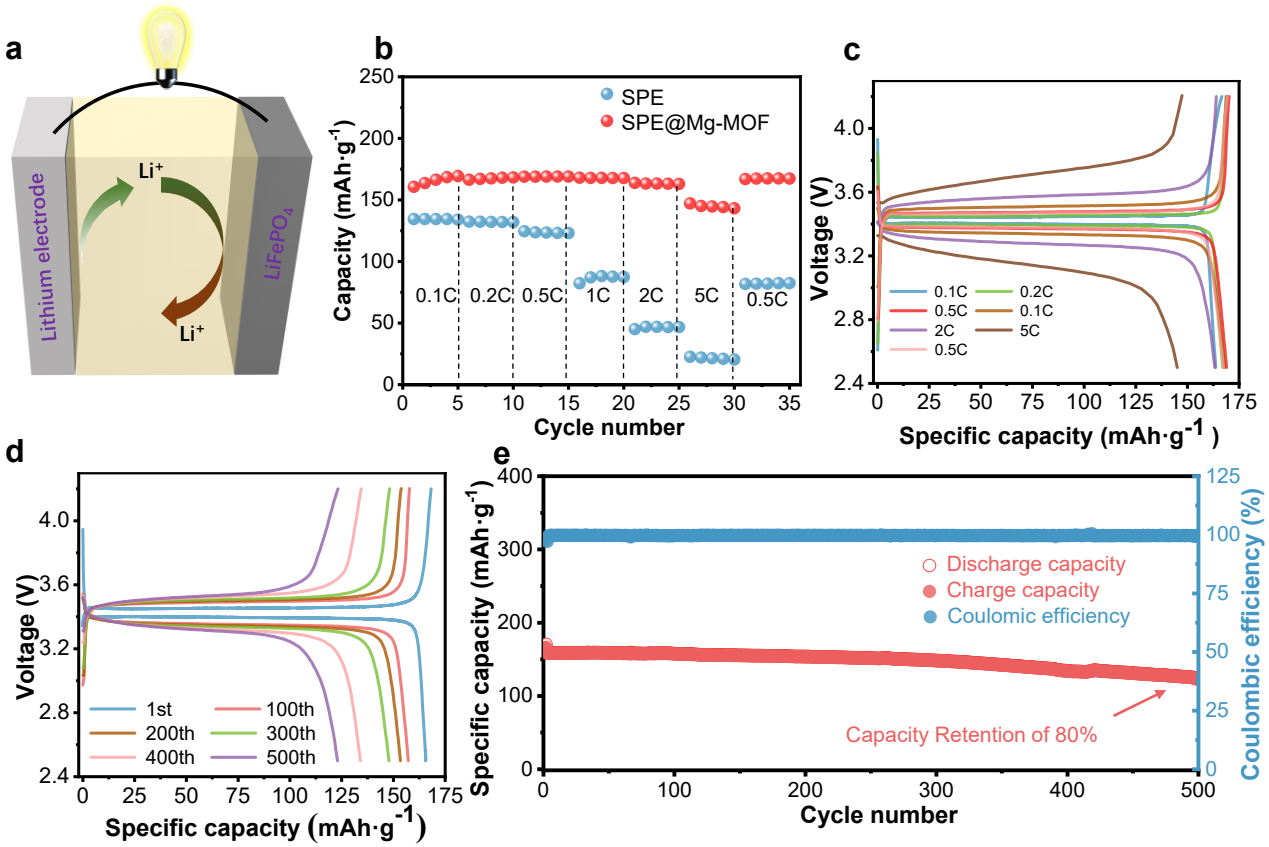

Fig. 5 **a** Schematic diagram of LFP/SPE@Mg-MOF/Li. **b** rate capability (0.1–5 C) with LFP/SPE@Mg-MOF/Li and LFP/SPE/Li operated 60 ℃. **c** Typical charge-discharge curves at different rates. **c** Charge-discharge curves during the cycling at 1C. **e** Cycle performance at 0.1 and 1 C.

TOC (Table of Content)